Interfacial kinematics and governing mechanisms under the influence of high strain rate impact conditions: numerical computations of experimental observations

R.N. Raoelison[1,2*], T. Sapanathan[2], E. Padayodi[1], N. Buiron[2] , M. Rachik[2]

[1] Université de Bourgogne Franche Comté, Université de Technologie de Belfort Montbéliard, IRTES EA 7274, 90100 Belfort, France
[2] Sorbonne universités, Université de technologie de Compiègne, Laboratoire Roberval, CNRS UMR-7337, Centre de recherche de Royallieu, CS 60319, 60203 Compiègne cedex, France

Corresponding author: Rija Raoelison[1] rija-nirina.raoelison@utbm.fr (+33 384583097)

Abstract

This paper investigates the complex interfacial kinematics and governing mechanisms during high speed impact conditions. A robust numerical modelling technique using Eulerian simulations are used to explain the material response of the interface subjected to a high strain rate collision during a magnetic pulse welding. The capability of this model is demonstrated using the predictions of interfacial kinematics and revealing the governing mechanical behaviours. Numerical predictions of wave formation resulted with the upward or downward jetting and complex interfacial mixing governed by wake and vortex instabilities corroborate the experimental observations. Moreover, the prediction of the material ejection during the simulation explains the experimentally observed deposited particles outside the welded region. Formations of internal cavities along the interface is also closely resemble the resulted confined heating at the vicinity of the interface appeared from those wake and vortex instabilities. These results are key features of this simulation that also explains the potential mechanisms in the defects formation at the interface. These results indicate that the Eulerian computation not only has the advantage of predicting the governing mechanisms, but also it offers a non-destructive approach to identify the interfacial defects in an impact welded joint.

Keywords: Interfacial kinematics, numerical simulation, wavy interface, jet formation, impact mechanics

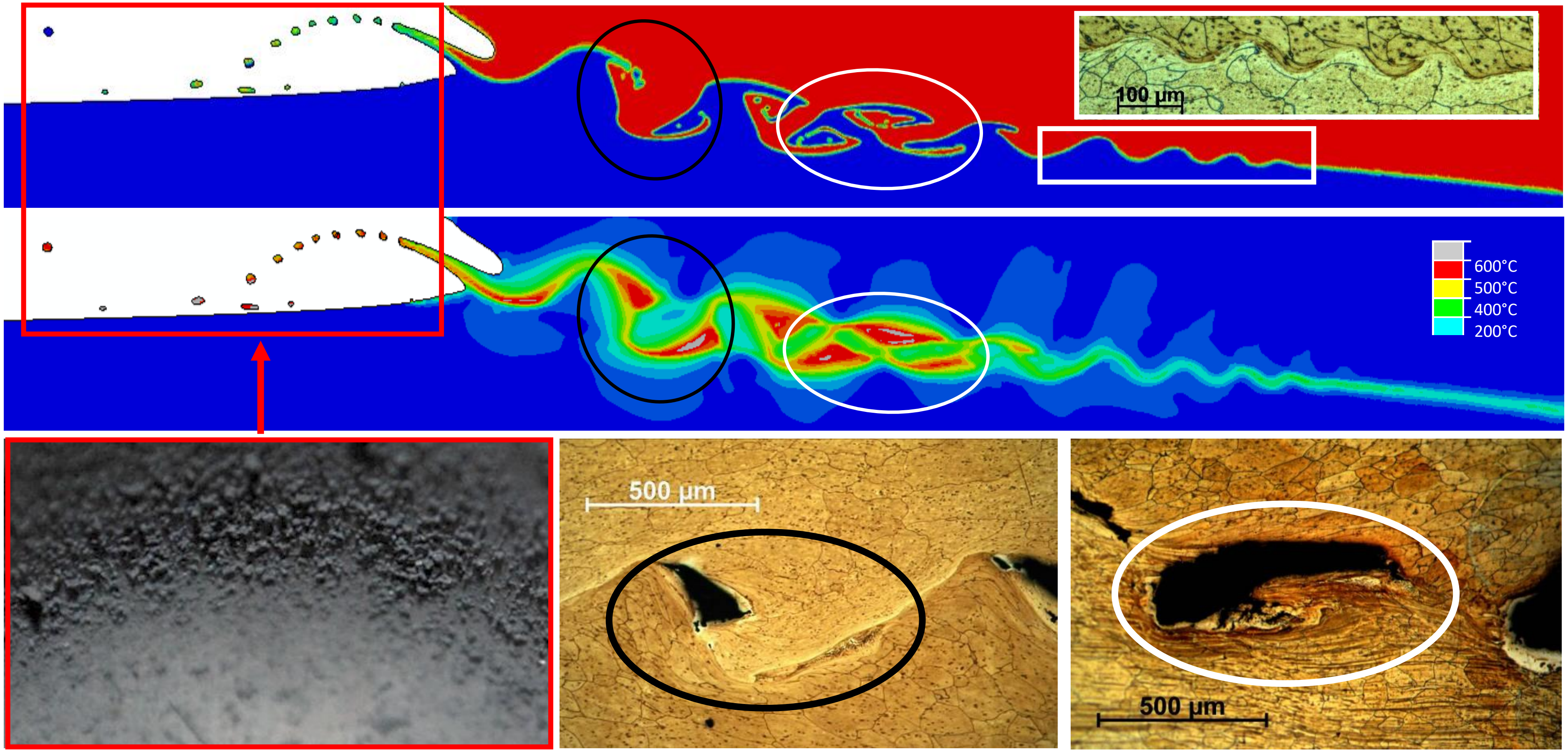

Abstract figure: Eulerian computation of interface behaviours during magnetic pulse welding.

1. Introduction

Adaptation of high speed joining techniques allows various possibilities to produce successful joints for similar and dissimilar metal combinations than several years ago. In the past, fusion welding was applied to metallurgically compatible materials, whose melting temperatures are similar to obtain successful joints. However, the new developments provide wide range of options to join metals with various melting temperatures, thus such welding methods eliminate the limitation of a fusion welding. In this way, the following welding methods become examples of high strain rate joining methods, viz., explosive welding [1], laser spot welding [2], magnetic pulse welding [3], vaporized foil actuator welding [4] and various friction welding process. Particularly those belong to high speed impact welding (HSIW), effectively utilizes the synergic effect of very high contact pressure in the range of 1-10 GPa and very short duration of the application time (i.e. a few hundred microseconds), thus these methods avoid the additional requirements of controlled heating or brazing. Using HSIW methods one could fabricate similar and dissimilar metal joints such as Cu/Brass, Cu/steel, Cu/Al, Al/steel, Ti/steel, Cu/Ti, Al/Mg, Al/Ni, Al/Fe, Al/Ti, Ti/Ni [3, 5-13] Cu/Zr metallic glass [14], Al/Zr-Cu metallic glass [15], Al/Fe metallic glass [16], Cu/Manganin [17], flexible circuit boards [18], W/CrCuZr [19], and multilayered dissimilar component; viz., Al/Cu/Al [20],Ti/mild steel/Ti [21] and Al/steel/Al [1].

The magnetic pulse welding (MPW) particularly has the advantages of flexibility, applicability, less requirement of energy due to short duration of process time, reduced cost, no requirements of consumables and environmental friendliness [22]. The Lorentz force generated as a result of electromagnetic impulse is effectively utilised to achieve successful collision for a MPW. It is also possible to obtain various coil designs for specific applications and which are capable of generating complex distribution of Lorentz forces [23]. According to a comprehensive review on this topic, the growing interest of this process is given by various industries, viz., automobile, aerospace, nuclear, electrical and microelectromechanical systems, ordnance and packaging while some of its applications are being industrialised [22]. Moreover, this process has various practical benefits and it is mainly suitable to fabricate tubular assemblies, flat shape connections and regular or irregular components. Although MPW has its unique characteristics, the interfacial behaviours and its interfacial kinematics are comparable to other HSIW processes [24-26].

During a HSIW, the notion of weldability is subjected to the complex interfacial kinematics. The interface morphology is mainly investigated to determine the formation of a successful joint. Generally, it is widely accepted that the formation of an interfacial wave produces a successful bonding; thus, various research studies were carried out to determine the favourable condition for such wave formation. Available theoretical literatures on this topic present the correlations between the material properties and dynamic interfacial parameters, based on analytical descriptions of the interface behaviour under hydrodynamic considerations. Various models were suggested to identify the onset of wavy pattern [27]. However, the existing analytical models are inadequate and reveal real difficulties of experimental conditions due to various factors. Those generic models do not include the high strain rate sensitivity of materials that governs the mechanical deformation and subsequent dynamic behaviour during the collision. Instead, those models include mechanical properties such as hardness and yield strength; and they generally rely on restrictive geometrical parameters that may lead to a poor representation of the real scenario and deviate from the real response of the interface [28-35]. Moreover, some other models are described by a set of dynamic parameters including collision velocity (collision propagation velocity) and dynamic collision angle (impact angle) whose real experimental values are very difficult to obtain at present [32-35]. Random evolutions of those parameters can also occur along the interface as the heterogeneous progression of the collision depending on the mechanical deformation of the interface. Furthermore, semi-empirical depictions of the weldability do not concur those analytical models. In a collision angle vs. collision velocity coordinate, the experimental lower limit can have an increasing downward curve [36-38] in contrast with the generic theoretical models. Danesh et al. have also considered a range of welding natures using several interfacial parameter sets (impact velocity, impact angle, normalized normal stress, specific pressure, deformation ration) and identify the important deviations with respect to experimental observations [39].

A recent theoretical investigation suggests more complex weldability ranges including specific influence on a coordinate system of inertia, time and pressure [28]. Many interface variances were also depicted to represent a 3D weldability range that consists of pre-critical zone (no welding), wavy zone (welding zone), waveless zone, anomalous wave zone, melt solidification zone, and supersonic zone [28]. Although, the pragmatic assessment of those analytical zone limits is defined by the collision angle and collision velocity, it again remains difficult as for the same reasons mentioned above. A reliable weldability depiction should include the multi-physics, kinematics and transient response of the interface during the collision. Under such conditions, the numerical simulation is a crucial and powerful tool that can assist to perform realistic virtual tests and predict the weld variance originated from the complex interface behaviour during the welding processes. In order to accomplish this purpose, this study proposes a computational method that enables to reproduce the interfacial characteristic changes. Prior to proceeding to the details of this method, this study also includes an assessment of the existing literatures on numerical simulations of high speed impact welding methods and summarizes them. These interfacial characteristics are identified as the main mechanisms those govern the experimentally revealed interfacial features. A discussion on the adequacy of the computational method is provided; then it highlights such interfacial characteristics and compares them in terms of complex interfacial kinematics and defects' morphology of welded interfaces.

2. Merits and limitations of existing impact welding simulations

Regarding the computation of weld formation during high speed impact welding processes, a limited literature is available and a part of which explains the interfacial conditions that produce either a successful weld or an adverse situation [40-43]. Mousavi et al. analysed several interfacial parameters including contact pressure, normal stress, shear stress, strain, impact velocity-dependant impact pressure, dynamic angle and temperature history [40, 44]. The authors also correlated those parameters and identify some bonding criteria, viz., jetting phenomenon, effective plastic strain, critical shear stress, interfacial wave formation, and collision velocities depending on the collision angle. Comparison with experimental observations also led to the suggestions of some other bonding criteria using a critical pressure and critical velocity, both depending on the effective strain at the onset of bonding [40, 44]. Furthermore, according to some other investigations, the interface should also experience the opposite shear stresses on both sides of the interface to form a successful bonding [42, 43, 45, 46]and vice versa, it is also argued that a same shearing orientation prevents the bonding. An experimental method to apprehend the bonding condition is unspecified since there exists a lack of practical recommendations, and particularly regarding the threshold value of the plastic strain required for a bonding. Nevertheless, the morphology of the interface remains the most reliable indicator to represent the weld variances that allows an accurate confrontation between experimental reality and computational results. In the literature, there have been various attempts to predict the wavy morphology using computational techniques. The capabilities and limitations of those computational methods are discussed below.

Lagrangian method is widely used to predict structural behaviour under mechanical dynamic loading, which relies on the deformation of a computational grid governed by the constitutive law of the material's response. With the grid deformation, Lagrangian computation produces a time dependant spatial kinematics. This method was found to be unsuitable for the simulation of impact welding because of the following reasons. Indeed, the high velocity collision generates a shear instability that activates the development of wavy morphology along the interface. Confined within wavy pattern, this instability phenomenon produces a large strain. Grains nearby the interface are also elongated and flattened as evidenced by several experimental observations [47, 48]. Therefore, method cannot fully reproduce such specific features due to the mesh distortion and deterioration when the shear instability appears. Lagrangian computation only provides an indication of jetting incident, and then quickly fails without the possibility to generate the wavy morphology [49, 50]. Alternatively, Adaptive Lagrangian-Eulerian (ALE) method has been used to prevent the mesh deterioration [51-53]. Throughout the computation, a remeshing procedure is enabled to perform node relocations that continuously facilitate to maintain the mesh quality throughout the simulation. Although, Nassiri et al. have implemented an ALE computation of impact welding, they investigated the interface morphology through a spatial disturbance analysis of velocity based on a stream-line formulation [51-53]. In another recent investigation, the authors have presented some results of ALE computation of the interfaces that are used to identify a welding range [51]. However, the credibility and effectiveness of the ALE procedure to compute the complex interfacial kinematics during an impact welding has not been clearly demonstrated, despite the considerations of precautious mesh refinement [51, 52]. In summary, the ALE simulation is most likely to produce a weakly wavy shaped interface.

The competences of meshless methods have brought new perspectives to the simulation of impact welding processes. In particular, molecular dynamics (MD) method can reproduce the phenomena of jetting, ejection, wave formation and vortex development [54-56]. However, MD is only suitable for small scales in the range of nanometres which restricts its capability of handling the simulation with a large scale structure. In order to perform a suitable confrontation between computation and experimental observation, Kiselev and Mali have suggested a dimensionless approach in a MD simulation [54, 55]. In their work, agreements with experiments are identified in terms of interface morphology and dimensionless jet velocity which is suggested to depend on Reynolds number (*Re*). The onset of jetting is identified by a specific *Re* value that requires as characteristic length the thickness of the jet rather than its length [55]. Those considerations of the MD method imply restrictions that make difficult to perform an accurate validation of the computation.

In contrast, meshless particle formulations, particularly the smooth particle hydrodynamics (SPH) method is less constraining to provide a relevant result. It allows simulating large strain cases of impact welding while solving the conservation equations of mass and momentum using a Lagrangian approach. The SPH method utilises a discrete method using a material particles formulation that relies on a kernel interpolation which approximates the field variables. The evolution of each state variable at each material particle is computed from the variable field of neighbouring particles. Therein, this method can capture the complex interface behaviours during an impact welding process including jetting, ejection and wave development [42, 43, 57, 58]. Potentials of the SPH method have also been considered even though its capability to accurately consider the dissipative terms is discussed [59]. Such physical phenomenon limits the use of SPH computation and makes it as an unviable solution.

In the literature of impact welding, a theory of fluid instability was suggested to explain the complex kinematics of the interface during the collision [60-62]. In a recent study, a symmetric sharp variation in tangential velocity associated with a jet-like plastic flow in a narrow sheared zone at the vicinity of the interface was claimed to cause the instability [63]. A fluid-like behaviour similar to that occurs during Kelvin-Helmholtz instability, which may cause the interfacial deformation and successive developments of humps and vortices within the localised zone; thus, suggesting a flow phenomenon that decides the interfacial feature such as the wavy morphology. The simulation of material flow has received a particular attention and the computational fluid dynamics can be used for that purpose. Abe has considered a different finite scheme with an elastic-plastic material and a symmetric collision to study the wavy interface generation, and then uses the isopynic distribution nearby the interface to reveal the interfacial waves [64, 65]. Moreover, when using an Eulerian formulation, the evolution of each state variable is computed in terms of transient variation and advection, the latter being a transport term which relates the material flow. A recent investigation has also considered utilizing the Eulerian computation that enables reproducing interfacial features resulted from high speed collision and the high strain rate nature of the process [66]. Although weak interfacial waves were computed, it has never been considered exploring the full capability of Eulerian method to produce the complex kinematics such as the full development of the wavy morphology along with the formation of vortices or defective welds, those scenarios have to be demonstrated. In order to accomplish this aspect, this paper presents Eulerian method to compute those typical complex weld variances and addresses a confrontation between experimental reality and virtual simulation results.

3. Experimental method and theoretical background of the numerical simulation

3.1 Experimental Method

3.1 Description of the Eulerian method

Eulerian method describes the time dependent state variables at any point of a domain while solving the conservation equations of mass, momentum and energy, respectively given by Eq. 1-3. The evolution of variables is computed on a fixed computational grid and the variables' history describes the response of the simulated media.

$$\frac{\partial \rho}{\partial t} + \vec{u}.\overrightarrow{grad(\rho)} = -\rho div(\vec{u}) \quad \text{(Eq. 1)}$$

$$\frac{\partial \vec{u}}{\partial t} + \vec{u}.\underline{\underline{grad(\vec{u})}} = \frac{1}{\rho}\overrightarrow{div\left(\underline{\underline{\sigma}}\right)} + \frac{1}{\rho}\overrightarrow{F_v} \quad \text{(Eq. 2)}$$

$$\frac{\partial e}{\partial t} + \vec{u}.\overrightarrow{grad(e)} = \underline{\underline{\sigma}}:\underline{\underline{D}} \quad \text{(Eq. 3)}$$

where, $\rho, \vec{u}, \underline{\underline{\sigma}}, \overrightarrow{F_v}, \underline{\underline{D}}, e$ respectively denotes density, velocity vector, Cauchy stress, internal body force vector, strain rate tensor and specific internal energy which is assumed to be an enthalpy to compute the dissipation of heat due to the plastic work $\underline{\underline{\sigma}}:\underline{\underline{D}}$.

Since a pure Eulerian computation is common in computational fluid dynamics, it has been widely exploited for both Newtonian and non-Newtonian fluids. However, for solids under non-linear dynamics conditions, the mechanical behaviour is governed by a high strain rate dependent stress that requires a constitutive law consideration including a hardening formulation and a numerical computation of plastic deformation in accordance with theory and numerical treatment of plasticity. For this purpose, a split strategy is suitable instead of the pure Eulerian method that directly computes the temporal evolution of state variables governed by the conservation equations (Eq. 1-3).

Therein split strategy suggests a separate computation of the transport term in the equations of mass, momentum and energy. Each conservation equation is decomposed into two parts using a generic formulation in Eq. 4.

$$\frac{\partial \emptyset}{\partial t} + \vec{u}.\overrightarrow{grad(\emptyset)} = f \qquad \text{(Eq. 4)}$$

The spilt forms of the generic formulation (Eq. 4) are given by Eq. 6 and 7.

$$\frac{\partial \emptyset}{\partial t} = f \qquad \text{(Eq. 6)}$$

$$\frac{\partial \emptyset}{\partial t} + \vec{u}.\overrightarrow{grad(\emptyset)} = 0 \qquad \text{(Eq. 7)}$$

where the usual equation of solid dynamics is expressed by Eq. 6 while the Eq. 7 corresponds to the advection (transport) of state variables. Thereby, the split method makes the possible treatment of solid constitutive law while applying the usual Lagrangian computation to the standard dynamic equation (Eq. 6). This is commonly known as the Lagrangian step. During this Lagrangian step, the mesh deformation is governed by the material behaviour that describes a structural deformation response due to the high strain rate dynamic constitutive law. The converged variable $\emptyset$ is then advected while directly solving Eq. 7 using the pure Eulerian method that is called the Eulerian step. Thereby, the variation of $\emptyset$ over time due to the advection is computed on a spatially fixed new mesh and produces a material flow (i.e. a transport phenomenon is treated as similar to a fluid flow). Eulerian step has the capability to accurately compute complex kinematics such as the interfacial instabilities of impact welding processes which are mostly interpreted using fluid like behaviours. A discrete formulation of Eq. 7 describes the progress of the state variables from old values. The computation uses the algorithm of Van Leer [67], a second order transport algorithm, that calculates the new values of the state variables at the middle of each elements of the new invariant mesh. Thus, a sequential computation of a Lagrangian step and an Eulerian step is used to reproduce the complex interfacial features found in magnetic pulse welding. For the sake of clarity, the transport algorithm can be described in its one dimensional form as follows:

$$\begin{gathered} \emptyset_{i+1/2}^{n+1} = \overline{\emptyset_{i+1/2}^{n}} + \frac{\Delta t}{\Delta x}\left(\Phi_i - \Phi_{i+1/2}\right) \\ with \;\; \Phi_i = \frac{u_{x\,i}}{2}\left(\emptyset_{i-1/2}^{n} + \overline{\emptyset_{i+1/2}^{n}}\right) + \frac{|u_{x\,i}|}{2}\left(\emptyset_{i-1/2}^{n} - \overline{\emptyset_{i+1/2}^{n}}\right) \\ and\; \overline{\emptyset_{i+1/2}^{n}} = \int_{x_i}^{x_{i+1}} \emptyset_{i+1/2}^{n}(x)\, dx \end{gathered} \qquad \text{(Eq. 8)}$$

where, the subscript i is the spatial location of the element (i.e. the i^{th} node). $i+1/2$ and $i-1/2$ respectively refer the middle of the current element and upwind adjacent element. The superscripts n and $n+1$ respectively denote the old and new values corresponding to the transport step.

3.2 Consideration of the material interface

Eulerian method in Abaqus/explicit utilises a volume of fluid (VOF) front tracking method to calculate the material interface. Each interfacial element can have either one or more materials or materials with some void space in a fixed mesh. In order to manipulate the interfacial materials, the initial volume fraction of each material, $C_{m,i}$, is calculated at the end of each Lagrangian step and then the advection uses these variables to transport into an Eulerian mesh. Initially, a zero volume fraction also assigned for the void materials. Generally, the total computed Eulerian volume fraction of all the materials should be equal to one (i.e. for n material case $\sum_{i=2,n} C_{m,i} = 1$). However, when the total volume fraction is smaller than one, it is filled by void material accordingly to its residual volume fraction. After that, these computed volume fractions are used to reconstruct the material interfaces and Eulerian material boundaries (material/void interface) using Young's algorithm [68]. The algorithm uses a simple line interface calculation (SLIC) method to reconstruct the interface with its phenomenological characteristics during the welding. Post-processing of the results also involves a smoothing nodal averaging method that further improves the regularity of the interface.

Albeit Eulerian method provides adequate evidence to determine the weldability window via reproducing the interfacial characteristics, it requires a sufficiently fine mesh to capture these features that demands for heavy computation. Moreover, it requires an adaptation of time step to overcome the flow of material across more than one element while performing the advection step; thus, the total computation time also increases. In this study, we use a mesh size of 5 μm at the proximity of the interface with a stable time step of 10^{-10} to 10^{-11}, set for the total computer time of 10 μs. The output results generated during the simulation also requires storage of several gigabytes. Beyond these requisites, the merits of this method for the impact welding simulations deserve to be fully investigated to numerically identify the weldability window of those processes. Furthermore, aforementioned requirements are easily manageable with high performance advanced computing technologies available to date.

4. Computational model specification

4.1 Mechanical behaviour and physical properties of materials

Johnson-Cook flow stress model implemented to capture the high strain rate deformation of the materials is described by Eq. 9.

$$\sigma_y = \left[A + B(\varepsilon_p)^n\right]\left[1 + Cln\left(\frac{\dot{\varepsilon_p}}{\dot{\varepsilon_{p0}}}\right)\right]\left[1 - \left(\frac{T - T_0}{T_m - T_0}\right)^m\right] \qquad \text{(Eq. 9)}$$

where, σ_y, ε_p, $\dot{\varepsilon_p}$, T are von Mises equivalent stress, strain, strain rate and temperature respectively. Moreover, Mie-Grüneisen's equation of state (EOS) is used to describe the variation in pressure according to the thermodynamics condition of the material. It is a pressure-density relation and the density is a state variable described by the equation of mass conservation. Material parameters corresponding to the Johnson-Cook equation (Eq. 9) and other material data used in the model are listed in Table 1 [69]. The materials are considered as isotropic and the von Mises criterion is used to describe the isotropic yield surface. The plastic normality rule governs the hardening computation throughout the entire simulation. While predicting the kinematics of the interface, the numerical simulations include an adiabatic heating resulted from the plastic deformation and the heating effect is prominent at the confined interface region due to severe interfacial shearing and collision. The physical behaviour of the air is not computed in the Eulerian simulations while VOF method performs the calculations for the volume of air domain in each mesh element in the dynamic explicit procedure in Abaqus 6.14, while these considerations also account for the geometric nonlinearity with large displacement of the interface.

Parameter	Name of the material property	Unit	Value
A	Yield strength	MPa	148
B	Hardening coefficient	MPa	345
C	Strain rate constant	-	0.001
C_0	Sound speed	m/s	5350
C_p	Specific heat capacity	J/(Kg.K)	900
E	Young's modulus	GPa	70
G	Shear modulus	GPa	26.2
m	Softening exponent	-	0.895
n	Strain hardening exponent	-	0.183
s	Slope of linear Rankine–Hugoniot's law	-	1.37
T_0	Reference temperature	K	298
T_m	Melting temperature	K	916

γ_0	Mie-Grüneisen's coefficient	-	2.14
$\dot{\varepsilon}_{p0}$	Reference strain rate	s^{-1}	1
ν	Poisson's ratio	-	0.33
ρ_0	Reference density	Kg/m^3	2700

Table 1. Material properties used in the numerical model for aluminium workpieces.

4.2 Geometrical considerations and boundary conditions

The schematic illustration in Fig. 1 shows, geometrical details and boundary conditions used in the simulations in an overlap configuration providing a tube with solid rod assembly. The out-of-plane degree of freedom (DOF) is not activated so that we obtain a 2D equivalent computational model. Thereby, the thickness of the domain can be arbitrarily chosen. The tube's length, inner diameter and outer diameter are respectively set as 43mm, 22mm and 25mm. The overlapping length and initial air gap between the workpieces are 10mm and 2mm respectively. Experimental observations indicate that the propagation of the weld is from the right to the left along the interface; hence, the numerical simulation was performed in the same direction. The flyer is assigned with a negative radial velocity in its overlapping zone. A linear distribution of V_y is considered with the mean value of about 600 m/s to generate and explain the complex interfacial instabilities which are caused by the physical phenomena during a typical impact welding. In order to estimate the exact velocity field, we proposed multi-physics simulation for the situation in the future. Since the experimental observations of magnetic pulse welded joints evidenced a bonded interface which experiences a large shear deformation on its both side. The grains nearby the interface are flattened and sheared with an excessive shearing without any apparent sliding at the interface itself [48]. A tangential sliding should limit or even prevent this shearing as experimentally evidenced. Thereby, the use of a normal contact behavior has been enacted in this paper.

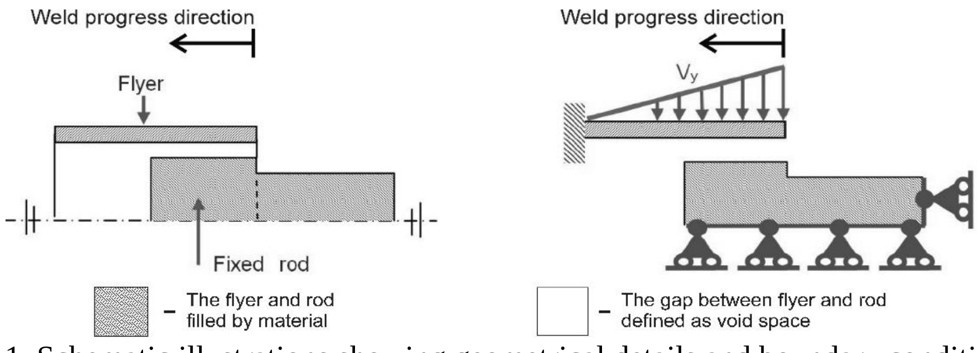

Fig.1. Schematic illustrations showing geometrical details and boundary conditions.

5. Simulation of interfacial kinematics during MPW

The Eulerian computation of the high strain collision produces a series of interfacial instabilities. Fig. 2 presents a development of interface while the collision progresses from the right to the left. Three distinct kinematic responses of the interfaces are distinguished; namely (1) a generation of wavy interface whose morphology evolves from a regular shape towards wake instability, (2) a vortex development forming a complex intermixed interface that experiences a confined heating and (3) an ejection phenomenon arising from thermomechanical flow of material combined with progressive jetting. Each one of that kinematics are discussed in the subsequent sections and compared to experimental observations.

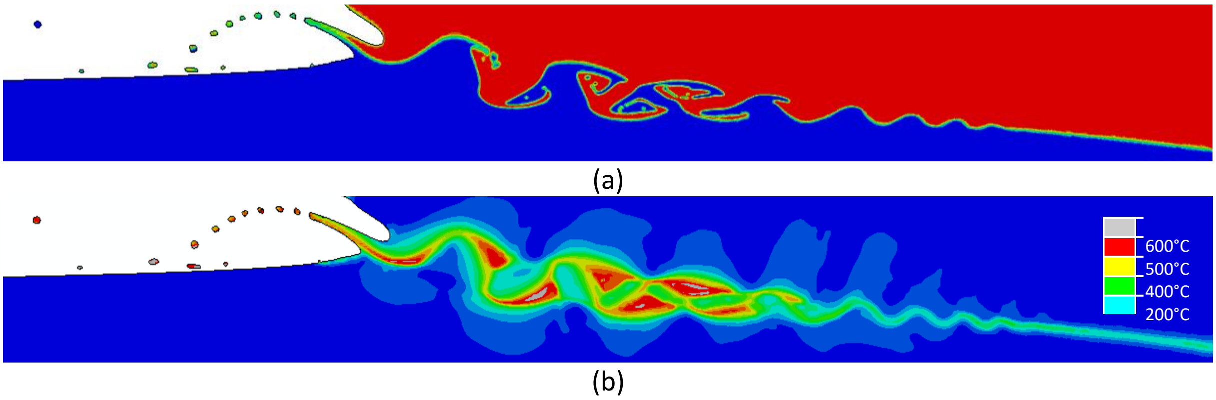

Fig. 2. Eulerian computation of the high strain rate progressive collision in an impact welding; (a) development of a series of complex kinematics and (b) thermomechanical response of the interface.

5.1 Interfacial instability: formation of wave and wake region

The transition of the interface morphology from a straight shape towards a wavy pattern represents the onset of instability kinematics in an impact welding. Fig. 3 shows the kinematics of wave generation while the collision evolves along the interface. The Eulerian computation provides an excellent description of the interface morphology since a clear transition from straight to wavy has been produced followed by the predictions of increase in wave heights. During the interfacial instability, intermittent upward and downward jetting produces the sequence of inverted curves along the interface (Fig. 3a-c). Thereby, the wavy pattern is periodically formed and the wave height gradually increases with the progression of the collision during which the upward jetting arises from the interfacial shear instability (Fig. 3d). An oblique collision produces a tangential velocity called collision velocity which causes the strong shear that produces the upward jetting. The downward jetting occurs with the impact propagation while the flyer subjected to the impact velocity progressively impinges onto the inner rod, from the left to the right direction.

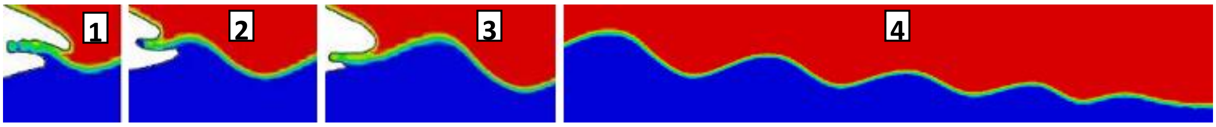

(a) (b) (c) (d)

Fig. 3. Eulerian simulation of the jetting kinematics during the collision propagation: onset of upward jet (a), onset of downward jet (b), complete downward jet followed by next upward jet (c), and development of the wavy interface (d).

The development of the wavy interface experiences a further interfacial instability. The interface experiences the kinematics with a distinguishable transition; thus, the regular shape of the wave evolves towards an irregularly nature. The shearing at the front and back side of the instable wave produces a wake regime which begins with the irregular deformation of the native wave. At both top of the front side and bottom of the back side of the native wave, ab initio of wake appears. The wake formation reaches a developed stage that exhibits an apparent wake flow. The successive wakes become larger than that of the previous one. This new instability marks a transition of a complex kinematics that is displayed in Fig. 4. The complex kinematics of the wake regime is produced with a fine description of the material interface. The Eulerian computation can provide accurate predictions with respect to the weld generation including the development of interfacial wavy morphology and wake during the progressive collision (Fig. 5).

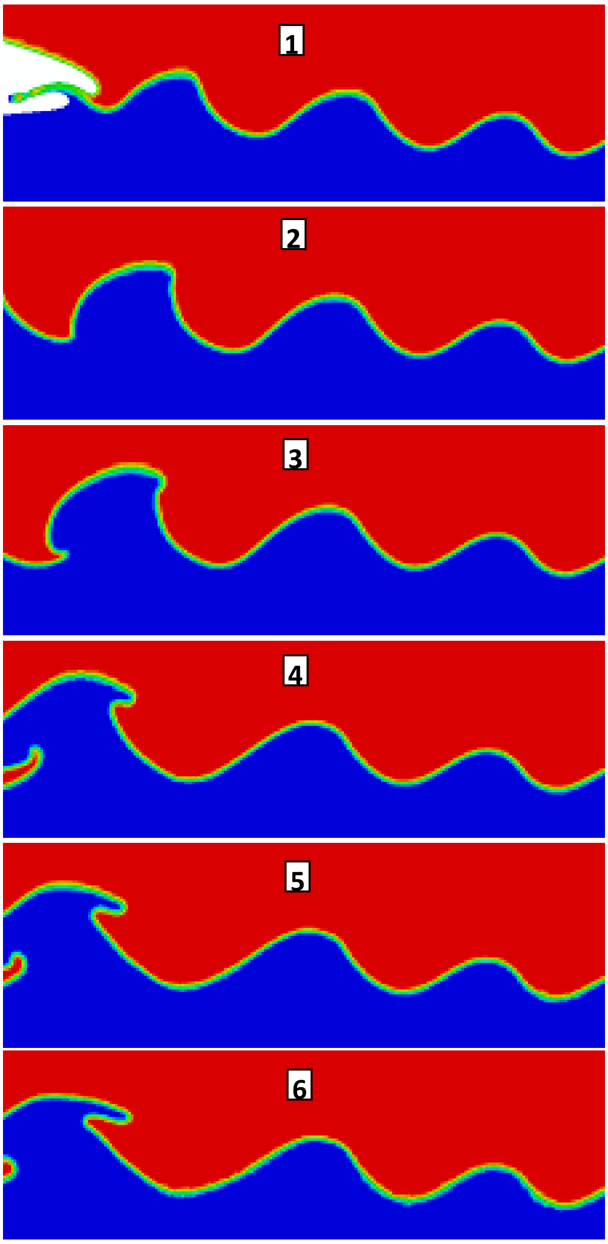

Fig. 4. Eulerian computation of a wake instability development

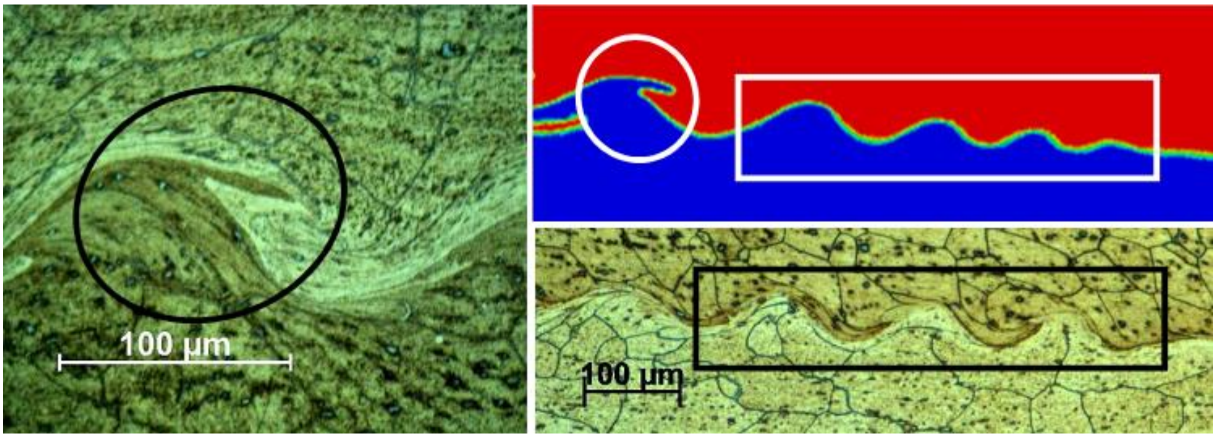

Fig. 5. Kinematic instability obtained from Eulerian computation and experimental means revealing the development of both interfacial wavy morphology and wake during the

progressive collision. Boxed and Circled regions respectively denote wavy formation and wake initiation.

5.2 Vortex development, interfacial mixing, and potential failure

In impact welding, the interface is believed to adopt a fluid-like behaviour that allows producing complex kinematics. During the interfacial instabilities, material flow creates various interfacial features which not only include the previous ones, but also bring specific characteristics due to the development of vortex instability. These kinematic instabilities can be classified into the widely known Kelvin-Helmholtz instability phenomena in fluids [31]; accordingly, the vortex formation starts at the wake affected zone (WAZ). The tangential velocity experienced by the moving flyer on the motionless fixed inner rod causes a swirling kinematic flow that forms the vortex. The interface material twists and locally rolls within the vortex similar to a fluidic motion (Fig .6). The two sides of the native interface become intermixed due to the vortex development. Such feature is observed at an early stage of a vortex formation as shown in Fig. 6, and particularly in the WAZ wake. When the vortex instability reaches an advanced stage, the swirling kinematics produces a real interfacial mixing. The strong kinematics within the vortex affected zone (VAZ) involves a strongly confined plastic work that promotes a significant local heating. Confinement of high temperature are observed whose value reaches 600°C, even exceeds this threshold (Fig. 7). Consequently, strong thermomechanical softening, even melting makes these zones vulnerable to a potential defect along the weld. The experimental observation of a defective weld concurs with the simulation. Firstly, a good agreement of the intermittent interface pattern is noticed. That is, the Eulerian computation reproduces the irregular pattern (Fig. 7) with an adequate indication of the potential zone of failure. Secondly, a noticeable agreement is found between the virtual defect and the experimental voids characterizing the defective weld. Using the temperature distribution as an indicator of defect, the simulation exhibits predictive defect shapes (Fig. 7), in addition to the genesis at the specific expected zone as previously mentioned.

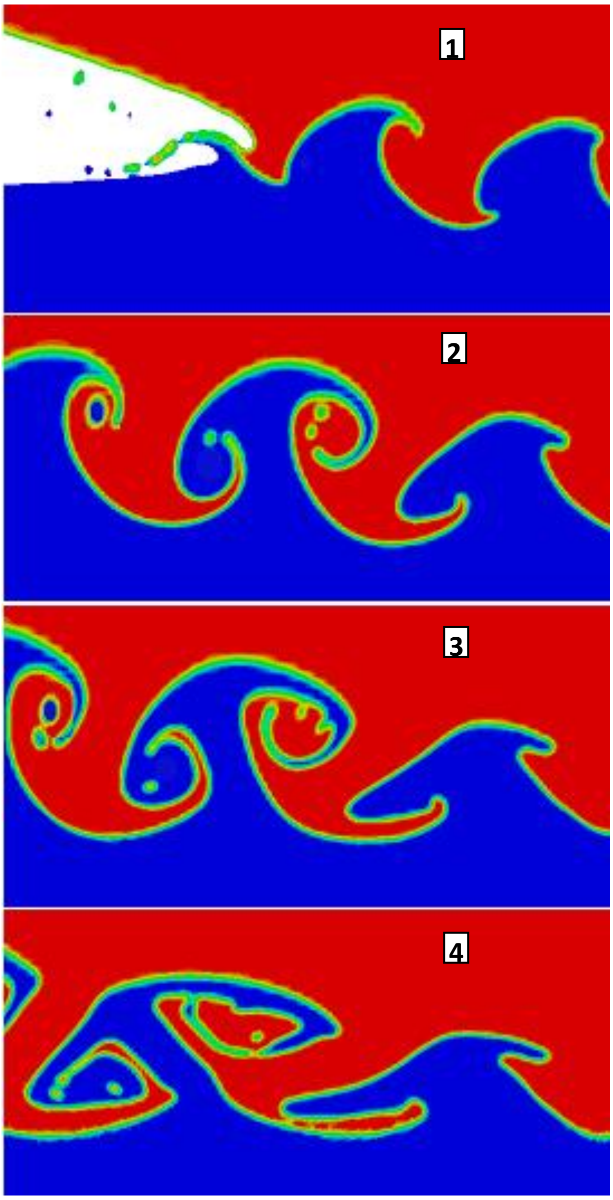

Fig. 6. Eulerian computation revealing the complex kinematics of vortices at the welded interface.

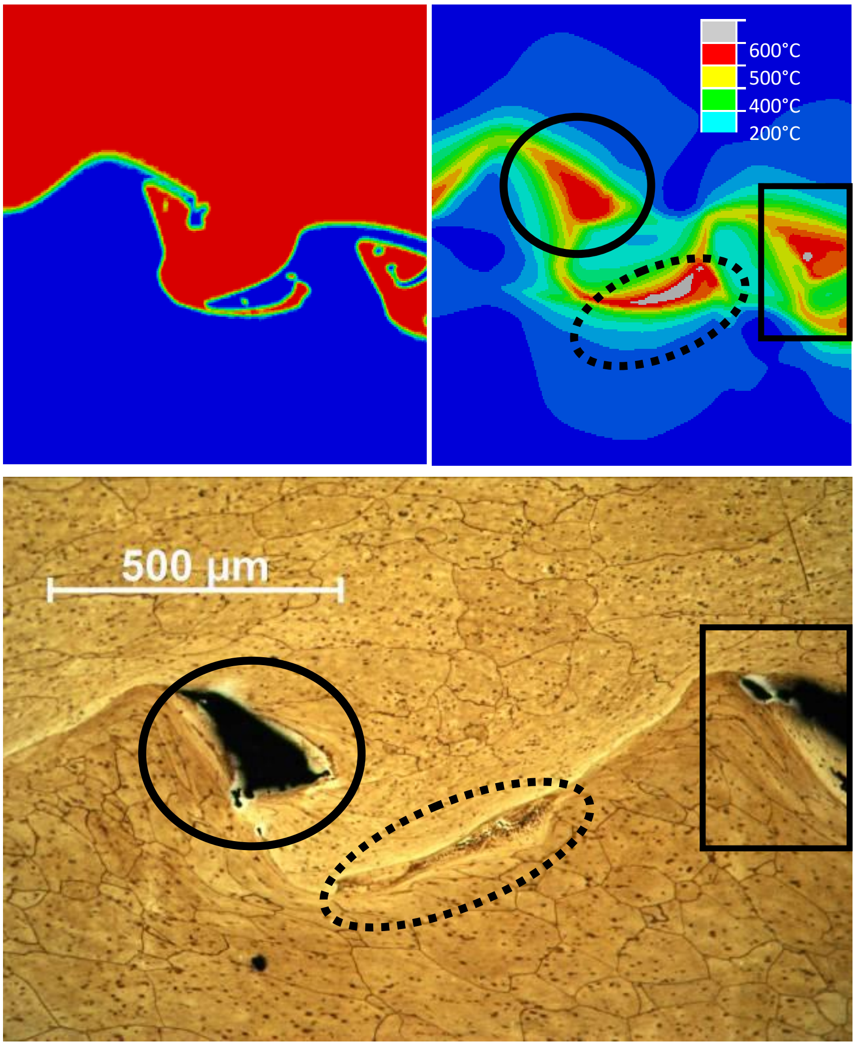

Fig. 7. Eulerian computation indicating heat confinement that represents the zones of potential failure where the regions corresponding to variously denoted objects (circles and square) are in agreement with experimental defects in terms of their shapes and locations.

The development of instability within the vortex site further complicates the intermixing flow at the interface. Due to the growth of VAZ, the interface morphology is become strongly heterogeneous with a material mixing, and the temperature distribution exhibits a strong non-uniformity. The zone affected by significantly high heat, increases and coalesces into a larger region of confined high temperature (Fig. 8). The comparison with an experimental observation indicates that this heat affected zone (HAZ) corresponds to a defect occurrence. The experimental defect is quite similar to the computed and coalesced HAZ in terms of both morphology and location (Fig. 8). A catastrophic failure of the HAZ, by ejection during the progressive collision, or by fragmentation during the surface preparation for the interface observation, or both, are the possible detrimental phenomena leading to the defective hole. Nevertheless, the aforementioned similarity allows stating the Eulerian computation of the complex interfacial kinematics and intermixing which provides a useful understanding of the situation of defects occurrence during the weld formation in a high speed collision welding process.

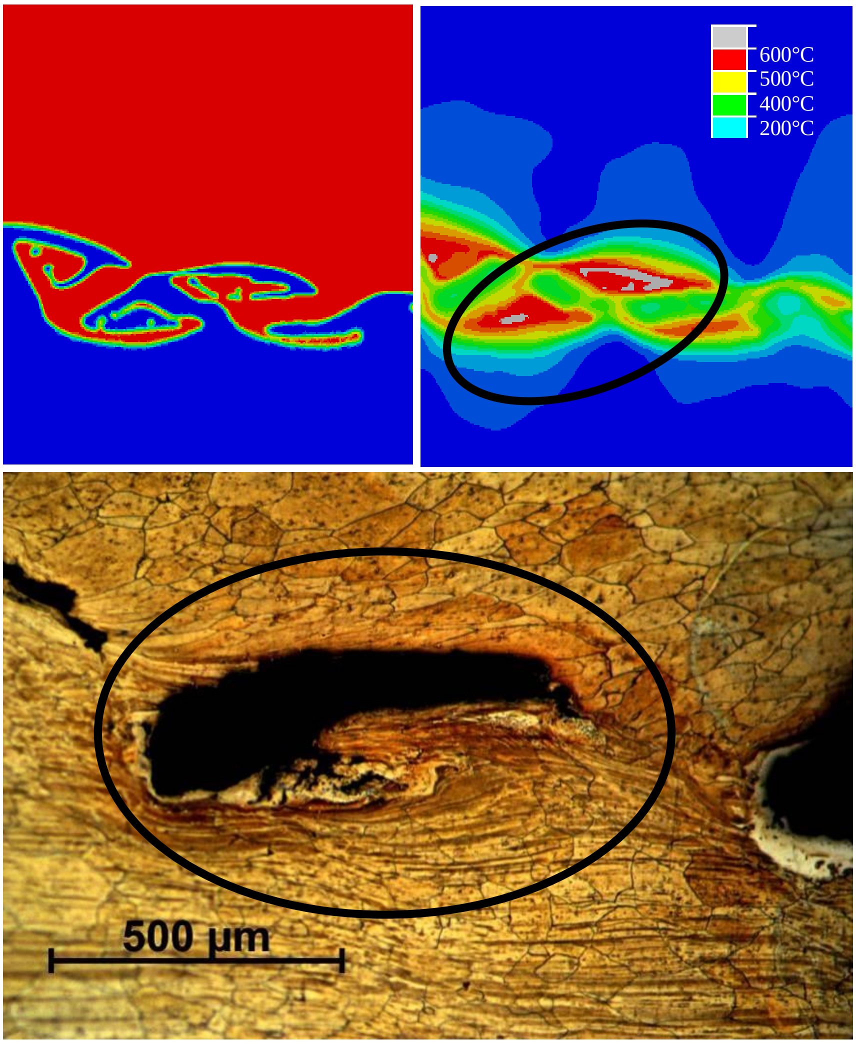

Fig. 8. Eulerian computation of a HAZ increases and coalesces into a larger region of confined high temperature. Comparison with an experimental observation showing that the experimental defect is comparable with the computed coalesced HAZ in terms of both morphology and its location.

5.3 Thermomechanical phenomenon of material ejection

Lastly, ejection of fragments from the welded interface is also an experimentally evidenced phenomenon and it is significantly prominent in the case defective welded joints which also contain discontinuous voids at their interfaces [41,42]. The observation displayed in Fig. 9 is a typical case of ejection showing dispersed ejected particles outside the overlapping zone. The ejection phenomenon computed by the Eulerian method emphasizes the physical reality of the simulation. The ejected particles arise from jetting ahead the progressive collision region that is subjected to the severe interfacial shearing (Fig. 9). The temperature of the expulsed materials is also high, almost close to the melting temperature of the aluminium, so that the thermomechanical softening combined with the ejection inertia is able to promote the disintegration of the ejected material into particles. The material flow in the air as obtained from Eulerian simulation gives the temperature and location of the ejected particles away from the developed interface until the point of collision. Despite the ejection simulation is a result of a pure flow computation, the observation of experimental particles residue accredits the suitability of the Eulerian method to provide evidential predictions.

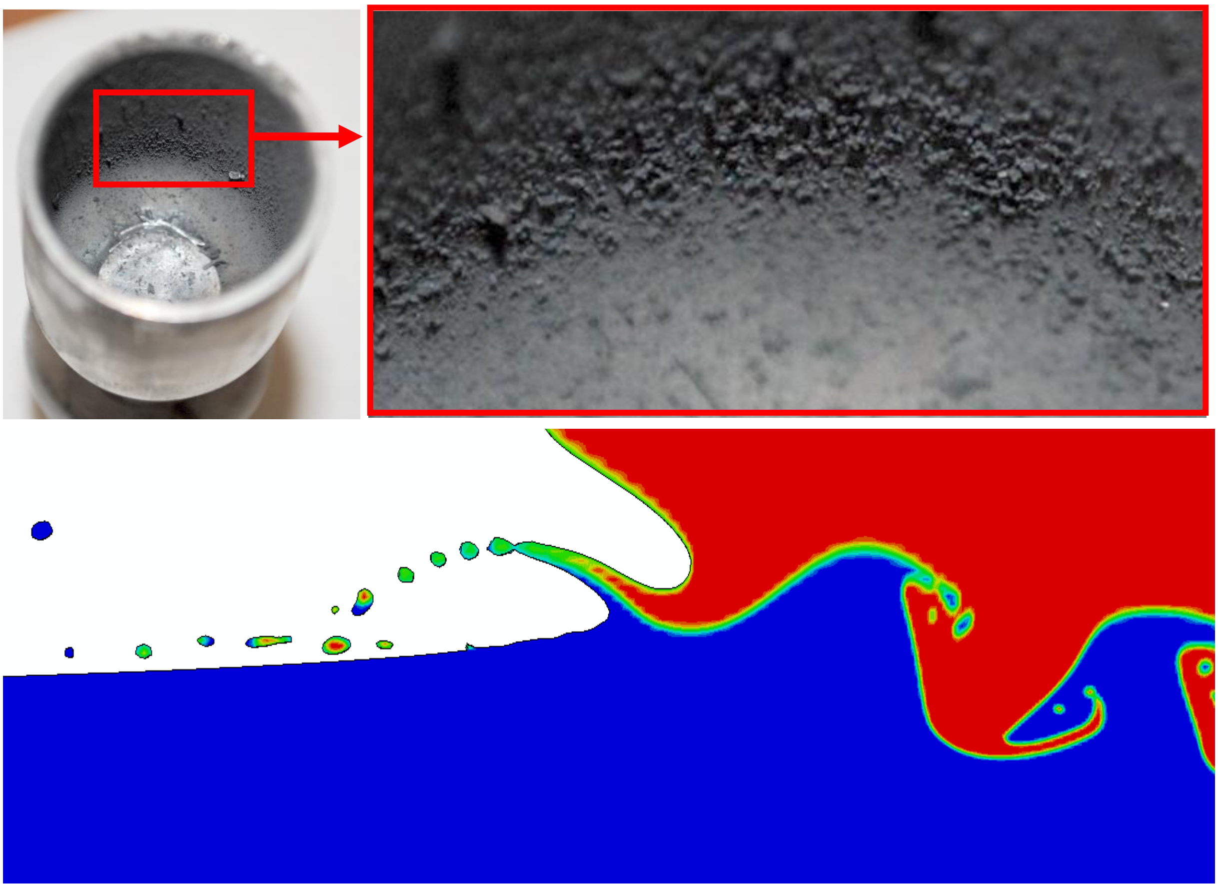

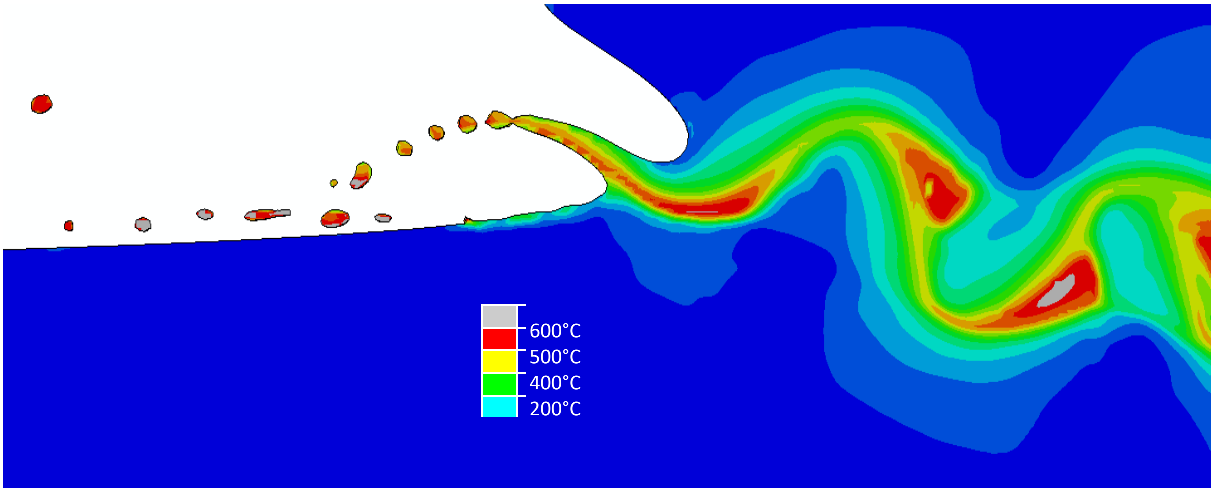

Fig. 9. Eulerian computation producing a physical realistic material jetting that explains the experimental observation of particles ejection from the interface.

5.4 Large strain and confinement plastic deformation at the interface region

A particular aspect of impact welding processes is the feature of the deformation produced by the high strain rate instability. The notion of shear instability is suggested to characterize those behaviours of the interface which begins by a shearing prior to the series of instability phenomena as previously mentioned, i.e., jetting, wave, wake, and vortices. During those instabilities, it was experimentally evidenced that the grains nearby the interfaces alone exhibit distinctive shear deformations. The grains neighbouring the interface region remain equiaxed, while the adjacent grains of the interface lose their initial equiaxed shape and become severely flattened and sheared. Such typical situation is shown in Fig. 10a which represents the onset of interfacial instability towards the transition from straight to wavy morphology. Fig. 10b highlights the confinement of this typical grain deformation during the development of the instabilities. The sheared grains form a zone with an excessive shearing state that characterizes the instabilities affected zone. This circumstance is clearly reproduced by the Eulerian computation. Along the interface, the deformation is confined at the interface and within the wavy pattern (Fig. 10c). The distribution of plastic strain indicates high values, mainly in the range of above 20% to 100%, showing thereby the computation of large strain in accordance with the experimental observations. From the straight to wavy transition zone towards the instabilities affected zone, the plastic strain remains at the confined immediate vicinity of interface. Therefore, the prevalent interfacial strain that characterizes the kinematic of instability during high strain rate impact welding processes can be accurately computed by the Eulerian simulation which is proven to have a real capability of physically realistic prediction.

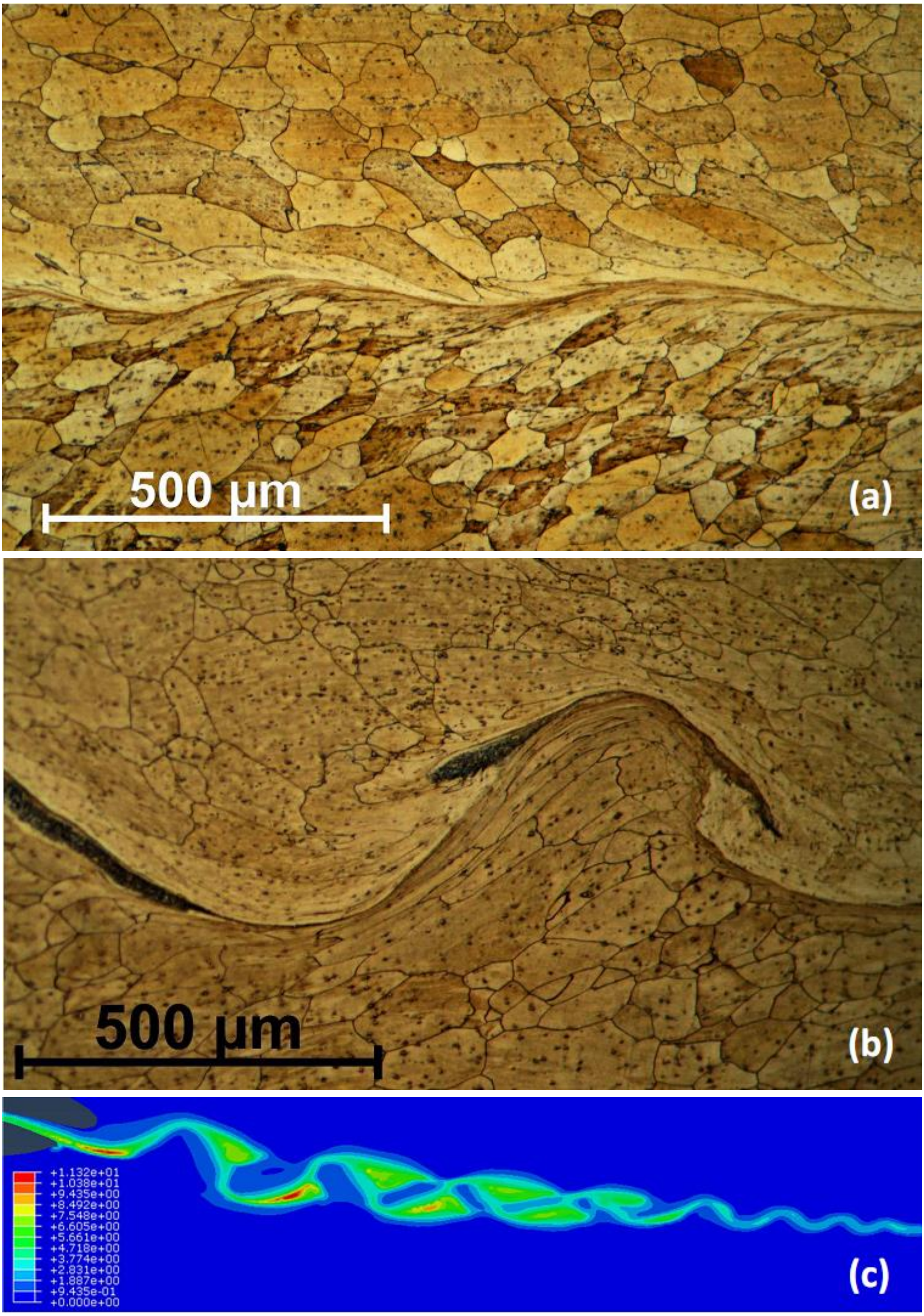

Fig. 10. Eulerian computation producing equivalent plastic strain mainly in the range of above 20% up to 100%, along the interface within those instabilities affected zones and physical

realistic comparison with experimental observation showing significantly large strain within the localised interface region.

6. Conclusions

Numerical simulations using an Eulerian method successfully reproduce the complex interfacial kinematics during high strain rate impact conditions. The predictions provide physical realistic evidences of the actual process behaviour. Convincing capabilities of the numerical model has been demonstrated. The Eulerian computation concurs with experimental observations and is suitable to:

- produce shear instability phenomenon including a jetting kinematics and consequent wave formation along the interface during the high strain rate collision,
- simulate complex interfacial mixing governed by a wake and vortex instabilities those lead to confined heating in those regions that evidence the formation of potential defects,
- compute the thermomechanical flow of material attributable to a particles ejection that can explain the experimental observation of ejected aggregates outside the overlapping zone.

These results clearly evidence the interfacial characteristics during high strain rate impact conditions as well as explain the governing mechanisms during the development of such characteristics. The convincing evidences and understandings of these governing mechanisms suggest the practical use of these simulation in virtual characterisation of high speed impact welding, thus it enables to inversely identify the weldability conditions.

References

[1] B. Gülenç, Y. Kaya, A. Durgutlu, İ.T. Gülenç, M.S. Yıldırım, N. Kahraman, Production of wire reinforced composite materials through explosive welding, Archives of Civil and Mechanical Engineering, 16 (2016) 1-8.
[2] X. He, P. Fuerschbach, T. DebRoy, Heat transfer and fluid flow during laser spot welding of 304 stainless steel, Journal of Physics D: Applied Physics, 36 (2003) 1388.
[3] V. Shribman, Magnetic Pulse welding for dissimilar and similar materials, in: 3rd International Conference on High Speed Forming, TU Dortmund, Dortmund, 2008, pp. 13-22.
[4] A. Vivek, B. Liu, S. Hansen, G. Daehn, Accessing collision welding process window for titanium/copper welds with vaporizing foil actuators and grooved targets, Journal of Materials Processing Technology, 214 (2014) 1583-1589.
[5] V. Shribman, Y. Livshitz, O. Gafri, Magnetic pulse welding and joining–a new tool for the automotive, SAE Technical Paper, (2001) 3401-3408.
[6] A.K. Jassim, Magnetic pulse welding technology, in: Energy, Power and Control (EPC-IQ), 1st International Conference, IEEE, Basra, 2010, pp. 363-373.
[7] F. Findik, Recent developments in explosive welding, Materials & Design, 32 (2011) 1081-1093.
[8] R. Raoelison, D. Racine, Z. Zhang, N. Buiron, D. Marceau, M. Rachik, Magnetic pulse welding: Interface of Al/Cu joint and investigation of intermetallic formation effect on the weld features, Journal of Manufacturing Processes, 16 (2014) 427-434.
[9] T. Baaten, N. Debroux, W. De Waele, K. Faes, Joining of copper to brass using magnetic pulse welding, in: 4th International Conference on High Speed Forming, Institut für Umformtechnik - Technische Universität Dortmund, Dortmund, 2010.
[10] R. Raoelison, M. Rachik, N. Buiron, D. Haye, M. Morel, B. Dos Sanstos, D. Jouaffre, G. Frantz, Assessment of gap and charging voltage influence on mechanical behaviour of joints obtained by magnetic pulse welding, in: 5th International Conference on High Speed Forming, Dortmund, 2012, pp. 207-216.
[11] H. Yu, Z. Xu, Z. Fan, Z. Zhao, C. Li, Mechanical property and microstructure of aluminum alloy-steel tubes joint by magnetic pulse welding, Materials Science and Engineering: A, 561 (2013) 259-265.
[12] R. Raoelison, N. Buiron, M. Rachik, D. Haye, G. Franz, Efficient welding conditions in magnetic pulse welding process, Journal of Manufacturing Processes, 14 (2012) 372-377.
[13] S. Mroz, G. Stradomski, H. Dyja, A. Galka, Using the explosive cladding method for production of Mg-Al bimetallic bars, Archives of Civil and Mechanical Engineering, 15 (2015) 317-323.
[14] N. Hutchinson, Y. Zhang, G. Daehn, K. Flores, Solid state joining of Zr-based bulk metallic glass, in: TMS 2009 Annual Meeting and Exhibition, TMS, San Francisco, 2009.
[15] M. Watanabe, S. Kumai, G. Hagimoto, Q. Zhang, K. Nakayama, Interfacial microstructure of aluminum/metallic glass lap joints fabricated by magnetic pulse welding, Materials transactions, 50 (2009) 1279-1285.
[16] W. Liu, K. Liu, Q. Chen, J. Wang, H. Yan, X. Li, Metallic glass coating on metals plate by adjusted explosive welding technique, Applied Surface Science, 255 (2009) 9343-9347.
[17] M. Kashani, T. Aizawa, K. Okagawa, Y. SUGIYAMA, Welding of Manganin and Copper sheets by Using Magnetic Pulse Welding (MPW) Technique, IEICE technical report EMD, 109 (2009) 29-31.
[18] T. Aizawa, K. Okagawa, M. Kashani, Application of magnetic pulse welding technique for flexible printed circuit boards (FPCB) lap joints, Journal of Materials Processing Technology, 213 (2013) 1095-1102.
[19] C. Sun, S. Wang, W. Guo, W. Shen, C. Ge, Bonding Interface of W–CuCrZr Explosively Welded Composite Plates for Plasma Facing Components, Journal of Materials Science & Technology, 30 (2014) 1230-1234.
[20] M. Sedighi, M. Honarpisheh, Experimental study of through-depth residual stress in explosive welded Al–Cu–Al multilayer, Materials & Design, 37 (2012) 577-581.

[21] D. Bae, Y. Chae, S. Lee, J. Lee, S. Park, Y. Lee, S. Lee, Effect of post heat treatment on bonding interfaces in Ti/Mild steel/Ti clad materials, Procedia Engineering, 10 (2011) 996-1001.
[22] A. Kapil, A. Sharma, Magnetic pulse welding: an efficient and environmentally friendly multi-material joining technique, Journal of Cleaner Production, 100 (2015) 35-58.
[23] V. Psyk, D. Risch, B.L. Kinsey, A.E. Tekkaya, M. Kleiner, Electromagnetic forming—A review, Journal of Materials Processing Technology, 211 (2011) 787-829.
[24] J. Verstraete, W. De Waele, K. Faes, Magnetic pulse welding: lessons to be learned from explosive welding, in: Sustainable Construction and Design 2011 (SCAD), Ghent University, Laboratory Soete, 2011, pp. 458-464.
[25] S.R. Reid, Wake instability mechanism for wave formation in explosive welding, International Journal of Mechanical Sciences, 20 (1978) 247-253.
[26] S.R. Reid, A discussion of the mechanism of interface wave generation in explosive welding, International Journal of Mechanical Sciences, 16 (1974) 399-413.
[27] M.H. Athar, B. Tolaminejad, Weldability window and the effect of interface morphology on the properties of Al/Cu/Al laminated composites fabricated by explosive welding, Materials & Design, 86 (2015) 516-525.
[28] V. Lysak, S. Kuzmin, Lower boundary in metal explosive welding. Evolution of ideas, Journal of Materials Processing Technology, 212 (2012) 150-156.
[29] J. Walsh, R. Shreffler, F. Willig, Limiting conditions for jet formation in high velocity collisions, Journal of Applied Physics, 24 (1953) 349-359.
[30] G.R. Cowan, A.H. Holtzman, Flow configurations in colliding plates: explosive bonding, Journal of applied physics, 34 (1963) 928-939.
[31] R. Wittman, The influence of collision parameters on the strength and microstructure of an explosion welded aluminum alloy, Proc. 2nd Sym. on Use of Explosive Energy in Manufacturing Metallic Materials of New Properties and Possibilities of Application thereof in the Chemical Industry, (1973) 153-168.
[32] A. Deribas, V. Simonov, I. Zakcharenko, Investigation of explosive welding parameters for arbitrary combinations of metals and alloys, in: Proc. 5th Int. Conf. on High Energy Rate Fabrication, 1975, pp. 1-4.1.
[33] B. Crossland, Explosive Welding of Metals and Its Application, Oxford University Press, London, 1982.
[34] V. Belayev, D. Devoino, V. Kasperovich, On the lower boundary of explosive welding modes, Poroshkovayametallurgiya, 2 (1978) 51-56.
[35] V. Shmorgun, On the evaluation of explosive welding efficient modes, Explosive Welding and Properties of Welded Joints. Inter-Departmental Transaction. Volgograd Polytechnic Institute, Volgograd, (1988) 68-74.
[36] Y. Zhang, S. Babu, G. Daehn, Impact welding in a variety of geometric configurations, in: 4th international conference on high speed forming, 2010, pp. 97-107.
[37] F. Grignon, D. Benson, K. Vecchio, M. Meyers, Explosive welding of aluminum to aluminum: analysis, computations and experiments, International Journal of Impact Engineering, 30 (2004) 1333-1351.
[38] E. Uhlmann, A. Ziefle, Modelling pulse magnetic welding processes–an empirical approach, in: 4th International Conference on High Speed Forming, Columbus, Ohio, USA, 2010, pp. 108-116.
[39] P. Dhanesh, S. Kore, P. Date, A numerical criterion for the formation of a solid state welded joint in sheets by electromagnetic forming/joining, in: 10th International Conference on Technology of Plasticity, Aachen, Germany, 2011, pp. 1154-1159.
[40] S.A. Mousavi, S. Al-Hassani, Finite element simulation of explosively-driven plate impact with application to explosive welding, Materials & Design, 29 (2008) 1-19.
[41] R. Alipour, F. Najarian, A FEM study of explosive welding of double layer tubes, World Academy of Science, Engineering and Technology, 73 (2011) 954-956.

[42] X. Wang, Y. Zheng, H. Liu, Z. Shen, Y. Hu, W. Li, Y. Gao, C. Guo, Numerical study of the mechanism of explosive/impact welding using Smoothed Particle Hydrodynamics method, Materials & Design, 35 (2012) 210-219.
[43] X. Wang, Y. Gu, T. Qiu, Y. Ma, D. Zhang, H. Liu, An experimental and numerical study of laser impact spot welding, Materials & Design, 65 (2015) 1143-1152.
[44] A.A. Mousavi, S. Burley, S. Al-Hassani, Simulation of explosive welding using the Williamsburg equation of state to model low detonation velocity explosives, International journal of impact engineering, 31 (2005) 719-734.
[45] S.A.A.A. Mousavi, Numerical studies of explosive welding of three-layer cylinder composites-part 2, in: Materials Science Forum, Trans Tech Publ, 2008, pp. 327-330.
[46] A.A. Mousavi, S. Al-Hassani, Numerical and experimental studies of the mechanism of the wavy interface formations in explosive/impact welding, Journal of the Mechanics and Physics of Solids, 53 (2005) 2501-2528.
[47] R. Raoelison, N. Buiron, M. Rachik, D. Haye, G. Franz, M. Habak, Study of the elaboration of a practical weldability window in magnetic pulse welding, Journal of Materials Processing Technology, 213 (2013) 1348-1354.
[48] R.N. Raoelison, T. Sapanathan, N. Buiron, M. Rachik, Magnetic pulse welding of Al/Al and Al/Cu metal pairs: Consequences of the dissimilar combination on the interfacial behavior during the welding process, Journal of Manufacturing Processes, 20, Part 1 (2015) 112-127.
[49] A. Nassiri, Investigation of wavy interfacial morphology in magnetic pulse welding: mathematical modelling, numerical simulation and experimental tests, in, Univseristy of New Hampshire, Durham, NH, 2005.
[50] A. Oberg, J. Schweitz, H. Olfsson, Computer modeling of the explosive welding process, in: Proceedings of the 8th International Conference on High Energy Rate Fabrication, San Antonio, Texas, 1984, pp. 75-84.
[51] A. Nassiri, G. Chini, B. Kinsey, Spatial stability analysis of emergent wavy interfacial patterns in magnetic pulsed welding, CIRP Annals-Manufacturing Technology, 63 (2014) 245-248.
[52] A. Nassiri, G. Chini, A. Vivek, G. Daehn, B. Kinsey, Arbitrary Lagrangian–Eulerian finite element simulation and experimental investigation of wavy interfacial morphology during high velocity impact welding, Materials & Design, 88 (2015) 345-358.
[53] A. Nassiri, G.P. Chini, B.L. Kinsey, Arbitrary Lagrangian Eulerian FEA Method to Predict Wavy Pattern and Weldability Window During Magnetic Pulsed Welding, in: ASME 2015 International Manufacturing Science and Engineering Conference, American Society of Mechanical Engineers, Charlotte, North Carolina, USA, 2015.
[54] S. Kiselev, V. Mali, Numerical and experimental modeling of jet formation during a high-velocity oblique impact of metal plates, Combustion, Explosion, and Shock Waves, 48 (2012) 214-225.
[55] S. Kiselev, Numerical simulation of wave formation in an oblique impact of plates by the method of molecular dynamics, Journal of Applied Mechanics and Technical Physics, 53 (2012) 907-917.
[56] O. Saresoja, A. Kuronen, K. Nordlund, Atomistic Simulation of the Explosion Welding Process, Advanced Engineering Materials, 14 (2012) 265-268.
[57] M. Liu, D. Feng, Z. Guo, A modified SPH method for modeling explosion and impact Problems, in: APCOM & ISCM, Scientech Publisher, Singapore, 2013.
[58] S. Kakizaki, M. Watanabe, S. Kumai, Simulation and experimental analysis of metal jet emission and weld interface morphology in impact welding, Materials transactions, 52 (2011) 1003-1008.
[59] D.J. Price, Smoothed particle hydrodynamics: things I wish my mother taught me, in: R. Capuzzo-Dolcetta, M. Limongi, A. Tornambè, G. Giobbi (Eds.) Advances in Computational Astrophysics: Methods, Tools, and Outcome, Astronomical Society of the Pacific, Cefalù, Italy, 2011.
[60] J. Hunt, Wave formation in explosive welding, Philosophical magazine, 17 (1968) 669-680.
[61] M.P.W. Wilson, J.H. Brunton, Wave Formation between Impacting Liquids in Explosive Welding and Erosion, Nature, 226 (1970) 538-541.

[62] J. Robinson, The mechanics of wave formation in impact welding, Philosophical Magazine, 31 (1975) 587-597.
[63] A. Nassiri, B. Kinsey, G. Chini, Shear instability of plastically-deforming metals in high-velocity impact welding, Journal of the Mechanics and Physics of Solids, 95 (2016) 351-373.
[64] A. Abe, Numerical Study of the Mechanism of Wavy Interface Generation in Explosive Welding, JSME International Journal Series B Fluids and Thermal Engineering, 40 (1997) 395-401.
[65] A. Abe, Numerical simulation of the plastic flow field near the bonding surface of explosive welding, Journal of Materials Processing Technology, 85 (1999) 162-165.
[66] W. Xu, X. Sun, Numerical investigation of electromagnetic pulse welded interfaces between dissimilar metals, Science and Technology of Welding and Joining, (2015) in press.
[67] Abaqus 6.14 Documentation, Dassault Systèmes Inc., Providence, RI, USA, 2014.
[68] D.L. Youngs, Time-dependent multi-material flow with large fluid distortion, Numerical methods for fluid dynamics, 24 (1982) 273-285.
[69] N. Gupta, M. Iqbal, G. Sekhon, Experimental and numerical studies on the behavior of thin aluminum plates subjected to impact by blunt-and hemispherical-nosed projectiles, International Journal of Impact Engineering, 32 (2006) 1921-1944.